Polymorphism and Phase Transition in Nanotubular Uranyl Phenylphosphonate: $(UO_2)_3(HO_3PC_6H_5)_2(O_3PC_6H_5)_2 \cdot H_2O$

Miguel A. G. Aranda,[†] Aurelio Cabeza,[†] Sebastian Bruque,*[,†] Damodara M. Poojary,[‡,§] and Abraham Clearfield[‡]

Departamento de Química Inorgánica, Cristalografía y Mineralogía, Universidad de Málaga, 29071 Málaga, Spain, and Department of Chemistry, Texas A & M University, College Station, Texas 77843

Received October 14, 1997

The synthesis and crystal structure of a new nanotubular phenylphosphonate, ϵ-$(UO_2)_3(HO_3PC_6H_5)_2(O_3PC_6H_5)_2 \cdot H_2O$, is reported. The compound crystallizes in the orthorhombic system, space group $P2_12_12_1$ with $a = 16.8268(7)$ Å, $b = 7.1673(8)$ Å, $c = 28.8228(12)$ Å, and $Z = 4$. The structure has been refined by the Rietveld method, and the final agreement factors were $R_{wP} = 13.1\%$ and $R_F = 10.1\%$. The structure of the ϵ-phase is very similar to that reported earlier for the δ-phase, and it consists of closed packed nanotubes. The main difference between δ- and ϵ-polymorphs is a slightly different interactions through the phenyl rings. The inside walls of these nanotubes are hydrophilic and the organic groups are projected outward, which results in hydrophobic regions between nanotubes. These nanotubes are held together only by van der Waals forces. The topotactic reversible phase transition between the two phases has been characterized by powder thermodiffractometry. ^{31}P MAS NMR data are also shown to display the structural relationship between both polymorphs.

Introduction

Metal phosphonates are hybrid organic−inorganic materials that can be conceived of as derivatives of the analogous metal phosphates by replacing an OH group of the phosphoric acid, H_2O_3P-OH, by an organic radical covalently bonded to the phosphorus atom, H_2O_3P-R (R = methyl, phenyl, or whatever organic radical). The crystal structures are usually lamellar formed by a central inorganic layer sandwiched by two organic layers.[1,2] However, other structures have been reported, and among them, microporous zeolite-like frameworks are outstanding examples[3−7] for future applications as molecular sieves.

The general interest in the chemistry of metal organophosphonates is mainly due to the unusual compositional and structural diversity which results in a wide range of applications. For example, it has important implications in electrochemistry,[8,9] microelectronics,[10] biological membranes,[11,12] photochemical mechanisms,[13,14] and catalysis.[15,16]

In the course of the research on uranyl phenylphosphonates, a number of phases have been reported. $[UO_2(HO_3PC_6H_5)_2(H_2O)]_2 \cdot 8H_2O$ (α-UPP)[17a] and $UO_2(HO_3PC_6H_5)_2 \cdot 2CH_3CH_2OH$ and its aqueous counterpart, $[UO_2(HO_3PC_6H_5)_2(H_2O)] \cdot 3H_2O$ (β-UPP),[17b] have crystal structures with linear chains. $UO_2(O_3PC_6H_5) \cdot 0.7H_2O$ has an entirely new structure containing one-dimensional tubular pores. The inside walls of these nanotubes are formed by the uranyl oxygens and the organic groups are projected out, resulting in isolated nanotubes held together only by van der Waals forces.[6] This compound is referred to as γ-UPP.[18] In other microporous phosphonates[3−5] the organic moieties are projected toward the center of the nanotubes. Finally, δ-$(UO_2)_3(HO_3PC_6H_5)_2(O_3PC_6H_5)_2 \cdot H_2O$ has a microporous structure related to that of γ-$UO_2(O_3PC_6H_5) \cdot 0.7H_2O$, but the metal−phosphonate linkages along the walls of the nanotubes are different. The nanotubes of δ-$(UO_2)_3(HO_3PC_6H_5)_2(O_3PC_6H_5)_2 \cdot H_2O$ are also held together only by van der Waals forces presenting a close packing. Each nanotube contains three crystallographically independent uranyl groups and four phosphonate groups, two of them protonated. The one-dimensional channel structure along the *b*-axis is formed by two U1−O−U2 infinite chains that share edges linked through a third uranyl group and the phosphonate moieties. The water is located approximately at the center of the hydrophilic nanotubes.[7]

* To whom correspondence should be addressed.
[†] Universidad de Málaga.
[‡] Texas A & M University.
[§] Current address: Symyx Technologies, 3100 Central Expressway, Santa Clara, CA 95051.

(1) Poojary, M. D.; Hu, H. L.; Campbell, F. L., III; Clearfield, A. *Acta Crystallogr.* **1993**, *B49*, 996−1001.
(2) Thompson, M. E. *Chem. Mater.* **1994**, *6*, 1168−1175.
(3) Le Bideau, J.; Payen, C.; Palvadeau, P.; Bujoli, B. *Inorg. Chem.* **1994**, *33*, 4885−4890.
(4) Maeda, K.; Akimoto, J.; Kiyozumi, Y.; Mizukami, F. *J. Chem. Soc., Chem. Commun.* **1995**, 1033−1034.
(5) Maeda, K.; Akimoto, J.; Kiyozumi, Y.; Mizukami, F. *Angew. Chem., Int. Ed. Engl.* **1995**, *34*, 1199−2001.
(6) Poojary, M. D.; Grohol, D.; Clearfield, A. *Angew. Chem., Int. Ed. Engl.* **1995**, *34*, 1508.
(7) Poojary, M. D.; Cabeza, A.; Aranda, M. A. G.; Bruque, S.; Clearfield, A. *Inorg. Chem.* **1996**, *35*, 1468−1473.
(8) Murray, R. W. *Accts. Chem. Res.* **1980**, *13*, 135−141.
(9) Facci, J. S. *Langmuir* **1987**, *3*, 525−530.
(10) Roberts, G. G. *Adv. Phys.* **1985**, *34*, 475−512.
(11) Ringsdorf, G.; Schmidt, X.; Schneider, J. *Thin Solid Films* **1987**, *152*, 207−222.
(12) Fendler, J. H. *Membrane Mimetic Chemistry*; Wiley: New York, 1982.
(13) Gratzel, M. *Pure Appl. Chem.* **1982**, *54*, 2369.
(14) Thomas, J. K. *Acc. Chem. Res.* **1988**, *21*, 275−280.
(15) Richard, M. A.; Deustsch, J.; Whitesides, G. M. *J. Am. Chem. Soc.* **1978**, *100*, 6613.
(16) Byrd, H.; Clearfield, A.; Poojary, M. D.; Reis, K. P.; Thompson, M. E. *Chem. Mater.* **1996**, *8*, 2239−2246.
(17) (a) Grohol, D.; Subramanian, M. A.; Poojary, M. D.; Clearfield, A. *Inorg. Chem.* **1996**, *35*, 5264−5271. (b) Grohol, D.; Clearfield, A. *J. Am. Chem. Soc.* **1997**, *119*, 4662.
(18) Grohol, D.; Clearfield, A. *J. Am. Chem. Soc.* **1997**, *119*, 9301.

S0020-1669(97)01294-9 CCC: $15.00
Published on Web 03/28/1998

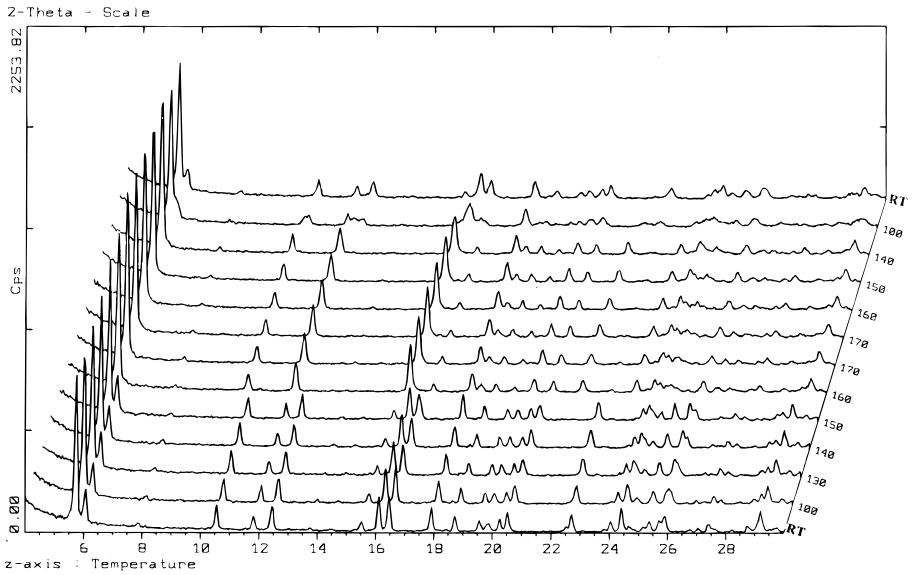

Figure 1. X-ray powder thermodiffractometry for δ-$(UO_2)_3(HO_3PC_6H_5)_2(O_3PC_6H_5)_2 \cdot H_2O$.

In this paper, we report a study of two very related microporous uranyl phosphonates: δ- and ϵ-$(UO_2)_3(HO_3PC_6H_5)_2(O_3PC_6H_5)_2 \cdot H_2O$. The crystal structure of the ϵ-phase has been determined from a Rietveld refinement of X-ray powder diffraction data. Powder thermodiffractometry and ^{31}P MAS NMR techniques have been used to characterize both polymorphs and the phase transition between them.

Experimental Section

Synthesis. Reagent quality chemicals were obtained from commercial sources and were used without further purification. ϵ-$(UO_2)_3(HO_3PC_6H_5)_2(O_3PC_6H_5)_2 \cdot H_2O$ (ϵ-UPP) was hydrothermally synthesized. A 50 mL volume of 0.1 M $UO_2(NO_3)_2$ solution was slowly added to 50 mL of 0.5 M $H_2O_3PC_6H_5$ solution with constant stirring (5:1 P:U molar ratio). The resulting yellow suspension was introduced into a Teflon-lined autoclave, sealed, and placed in an oven at 160 ± 10 °C for 4 days. The yellow solid was washed with water, then with acetone, and air-dried. δ-$(UO_2)_3(HO_3PC_6H_5)_2(O_3PC_6H_5)_2 \cdot H_2O$ (δ-UPP) was synthesized as previously reported.[7]

The uranium content was determined gravimetrically. The sample was dissolved in aqueous nitric acid solution (1:1), and the metal was precipitated as uranyl oxinate, which was then calcined at 900 °C to yield U_3O_8. The H and C contents were determined by elemental analysis in a Perkin-Elmer 240 analyzer. The P content was not determined, but it was calculated from the amount of carbon and by the known P:C ratio in phenylphosphonic groups of 1:6. The water content was determined from the weight loss in TGA. Anal. Calcd for $(UO_2)_3(HO_3PC_6H_5)_2(O_3PC_6H_5)_2 \cdot H_2O$: U, 49.11; P, 8.53; C, 19.81; H, 1.65; H_2O, 1.24. Found for ϵ-UPP: U, 50.2; P, 7.8; C, 18.1; H, 1.5; H_2O, 1.5.

X-ray Powder Data Collection. Room-temperature X-ray powder diffraction data were recorded for ϵ-UPP on a finely ground sample side-loaded into a flat aluminum sample holder using a Rigaku diffractometer. The X-ray source was a rotating-anode generator operating at 50 kV and 180 mA with a copper target and graphite monchromator, wavelengths Cu $K\alpha_{1,2}$. A 0.5° divergence and scatter slits and 0.15° receiving slit were employed. Data were collected in the 3−85° 2θ range, with 0.01° of step size and 10 s of counting time.

The powder thermodiffractometric study of δ-UPP was carried out in a Siemens D-5000 diffractometer equipped with a HTK10 heating chamber, wavelengths Cu $K\alpha_{1,2}$. The patterns were scanned in the 4−30° 2θ range, with 0.05° step size and 1 s counting time. Data were collected between room temperature and 170 °C, and the appropriate heating and cooling temperatures were selected by using the Diffract AT software. A delay time of 10 min, before each pattern, was used to allow the transformations may take place.

^{31}P MAS NMR Study. The spectra for δ- and ϵ-UPP were recorded at 121.4 MHz, with a Bruker MSL-300 spectrometer. The measurements were carried out at room temperature, and the samples were spun around the magic angle (54° 44′ with respect to the magnetic field) at spinning rate of 3.5 kHz. The ^{31}P chemical shift values are given relative to 85% H_3PO_4 aqueous solution.

Results

Thermodiffractometric Study. The thermal behavior of δ-UPP was recently reported,[7] and a phase transition at 152 °C was detected as an endotherm in the DTA curve without associated mass loss in the TGA curve. ϵ-UPP has a similar thermal behavior at high temperature (above 200 °C) but without the phase transition at ≈150 °C. The final thermal decomposition products of both polymorphs are a mixture of $^1/_3$ of UP_2O_7 and $^2/_3$ of $U(UO_2)(PO_4)_2$.

A thermodiffractometric study was undertaken to characterize the phase transition. In Figure 1 is shown the powder diffraction patterns upon heating and subsequent cooling. A phase transition close to 150 °C is clearly observed. The powder pattern of the high-temperature form coincides with that of ϵ-UPP obtained by direct synthesis at room temperature (see below). Hence, it can be concluded that δ-UPP transforms on heating to ϵ-UPP. The transition is reversible, and on cooling in these conditions, δ-UPP is obtained again.

Structural Study. The room-temperature powder diffraction pattern of ϵ-UPP was auto indexed by using TREOR90[19] in an orthorhombic unit cell. The result was a = 16.795(12) Å, b = 7.167(17) Å, c = 28.795(22) Å, V = 3466 Å^3, Z = 4, and V_{at} (non-hydrogen atom) = 17.3 Å^3/at, with a figure of merit, M_{20} = 10.[20] The unit cell parameters are very similar to those determined for δ-UPP[7] (a = 17.1966(2) Å, b = 7.2125(2) Å, c = 27.8282(4) Å, V = 3429 Å^3, Z = 4, and V_{at} = 17.1 Å^3/at). The systematic absences are consistent with the $P2_12_12_1$ in both compounds. Due to the similarities in the cell parameters of both phases and the relation found in the powder thermodiffractometric study (given above), the crystal structure of these polymorphs must be very related. Hence, we used the previ-

(19) Werner, P. E.; Eriksson, L.; Westdahl, M. *J. Appl. Crystallogr.* **1985**, *18*, 367−370.

Table 1. Positional Parameters for ϵ-$(UO_2)_3(HO_3PC_6H_5)_2(O_3PC_6H_5)_2{\cdot}H_2O$ in Space Group $P2_12_12_1$

atom	*x*	*y*	*z*
U1	0.6064(4)	0.2680(25)	0.1352(2)
U2	0.5093(4)	0.2682(25)	0.3790(2)
U3	0.3203(5)	0.3808(22)	0.2250(3)
P1	0.429(1)	0.286(3)	0.110(1)
P2	0.331(1)	0.271(3)	0.351(1)
P3	0.716(1)	0.364(3)	0.350(1)
P4	0.782(2)	0.308(6)	0.212(1)
O1	0.472(1)	0.100(3)	0.120(1)
O2	0.373(2)	0.341(5)	0.150(1)
O3	0.493(1)	0.441(3)	0.103(1)
O4	0.384(2)	0.447(3)	0.357(2)
O5	0.302(2)	0.251(6)	0.301(1)
O6	0.380(1)	0.098(3)	0.366(2)
O7	0.733(2)	0.208(4)	0.314(1)
O8	0.637(2)	0.328(5)	0.376(2)
O9	0.716(2)	0.557(4)	0.327(1)
O10	0.744(4)	0.122(6)	0.229(1)
O11	0.734(3)	0.392(8)	0.172(2)
O12	0.793(3)	0.454(7)	0.251(1)
O13	0.633(3)	0.237(8)	0.076(1)
O14	0.554(4)	0.302(2)	0.188(1)
O15	0.534(5)	0.294(6)	0.302(1)
O16	0.504(5)	0.274(5)	0.440(1)
O17	0.217(1)	0.346(9)	0.224(3)
O18	0.424(1)	0.393(22)	0.232(3)
O(w)	0.563(5)	0.556(11)	0.256(2)
C1	0.370(2)	0.263(7)	0.057(1)
C2	0.308(2)	0.387(7)	0.051(2)
C3	0.273(3)	0.403(12)	0.008(2)
C4	0.309(4)	0.318(12)	−0.030(1)
C5	0.384(4)	0.241(12)	−0.025(1)
C6	0.406(3)	0.184(12)	0.019(1)
C7	0.246(2)	0.294(8)	0.389(1)
C8	0.252(2)	0.253(14)	0.435(1)
C9	0.185(3)	0.215(13)	0.461(2)
C10	0.111(3)	0.255(11)	0.442(2)
C11	0.104(2)	0.297(11)	0.396(2)
C12	0.178(2)	0.329(16)	0.370(2)
C13	0.796(2)	0.361(5)	0.393(1)
C14	0.805(3)	0.513(7)	0.422(1)
C15	0.836(4)	0.486(12)	0.466(1)
C16	0.883(4)	0.331(12)	0.474(1)
C17	0.881(4)	0.184(10)	0.443(2)
C18	0.833(4)	0.195(7)	0.404(2)
C19	0.881(2)	0.250(11)	0.197(1)
C20	0.920(3)	0.379(15)	0.163(2)
C21	1.001(3)	0.361(21)	0.156(2)
C22	1.045(2)	0.248(25)	0.186(3)
C23	1.006(4)	0.118(22)	0.213(3)
C24	0.923(4)	0.112(15)	0.213(2)

ously determined crystal structure of δ-UPP[7] as a starting model for a Rietveld[21,22] refinement using the GSAS set of programs.[23]

The refined 2θ range was 7−50° as the high-angle part of the pattern (50−85°) has very strong overlapping with only some broad and diffuse bands. Due to irregularities in the background of the pattern, this was fitted manually and it was not refined. The common overall parameters, histogram scale factor, unit cell parameters, zero-shift error, and pseudo-Voigt coefficients[24] corrected for asymmetry,[25] were refined. As in δ-UPP, preferred

Table 2. Bond Distances (Å) for ϵ-$(UO_2)_3(HO_3PC_6H_5)_2(O_3PC_6H_5)_2{\cdot}H_2O$[a]

U1−O1	2.56(2)	U2−O1	2.40(2)
U1−O3	2.47(2)	U2−O3	2.41(3)
U1−O4	2.32(2)	U2−O4	2.54(4)
U1−O6	2.38(2)	U2−O6	2.53(2)
U1−O11	2.55(5)	U2−O8	2.20(3)
U1−O13	1.77(1)	U2−O15	1.77(1)
U1−O14	1.77(1)	U2−O16	1.77(1)
U3−O2	2.35(2)	U3−O10	2.43(4)
U3−O5	2.39(3)	U3−O17	1.76(1)
U3−O7	2.75(3)	U3−O18	1.76(1)
U3−O9	2.82(2)		
P1−O1	1.54(1)	P2−O4	1.55(1)
P1−O2	1.53(1)	P2−O5	1.54(1)
P1−O3	1.56(1)	P2−O6	1.55(1)
P1−C1	1.82(1)	P2−C7	1.81(1)
P3−O7	1.55(1)	P4−O10	1.56(1)
P3−O8	1.55(1)	P4−O11	1.54(1)
P3−O9	1.54(1)	P4−O12	1.55(1)
P3−C13	1.81(1)	P4−C19	1.82(1)

[a] Phenyl ⟨C−C⟩ = 1.38(1) Å.

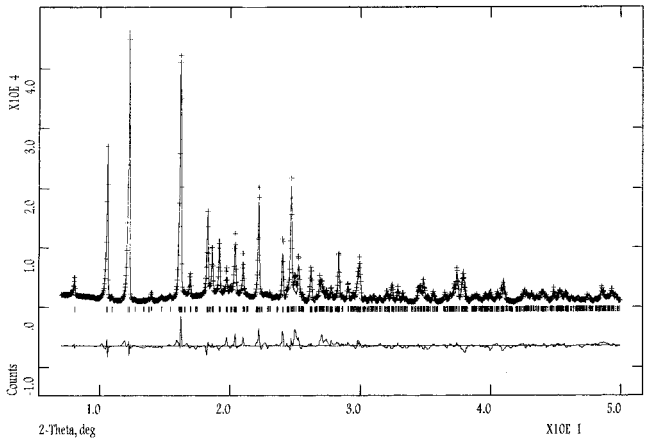

Figure 2. Rietveld refinement plot for ϵ-$(UO_2)_3(HO_3PC_6H_5)_2(O_3PC_6H_5)_2{\cdot}H_2O$.

orientation along the [010] axis and anisotropic peak broadening along this direction was also refined. After convergence, R_{wP} was 23.3%. At this stage, observation of the pattern, indicated that (00*l*) peaks had more observed intensity than the calculated from the starting structure. Hence, the preferred orientation was also refined along the [001] direction and R_{wP} fell to 18.6%.

This is a highly complex structure with 50 non-hydrogen atoms in general positions. Due to this complexity, the overlapping of the peaks, and the limited refined region, the use of soft constraints was imperative. However, for structures with well-known covalently bonded fragments, to use soft constraints is fully justified as it utilizes the vast crystallochemical information obtained in previous structural studies. The tetrahedral geometry around the P atoms was ensured through the following soft constraints: P−O 1.53(1) Å, P−C 1.80(1) Å, O···O 2.55(1) Å, and O···C 2.73(1) Å. To guarantee the well-known planar regular geometry of the phenyl groups, we used the following: C−C 1.380(5), C···C 2.39(1) Å, C·····C 2.76(1), and P···C 2.77(1) Å. The uranyl groups oxygen atoms were also constrained: U−O 1.76 (1) Å and O···O 3.52(1) Å. After refinement of the positional parameters with the highest damping factor, some oxygens in the polyhedron that surround the uraniums moved too close together. In these cases, new soft constraints [O···O 2.70(2) Å] were inserted inside the UO_7 groups. Isotropic temperature factors were set to 0.005 Å^2 for U, 0.01 Å^2 for P, 0.015 Å^2 for O, and 0.025 Å^2 for C, and they

(20) Wolff, P. M. *J. Appl. Crystallogr.* **1968**, *1*, 108−113.
(21) Rietveld, H. M. *J. Appl. Crystallogr.* **1969**, *2*, 65−71.
(22) Young, R. A. *The Rietveld Method*; Oxford University Press: Oxford, U.K., 1993.
(23) Larson, A. C.; von Dreele, R. B. Los Alamos National Lab. Rep. No. LA-UR-86-748, 1994.
(24) Thompson, P.; Cox, D. E.; Hasting, J. B. *J. Appl. Crystallogr.* **1987**, *20*, 79.
(25) Finger, L. W.; Cox, D. E.; Jephcoat, A. P. *J. Appl. Crystallogr.* **1994**, *27*, 892.

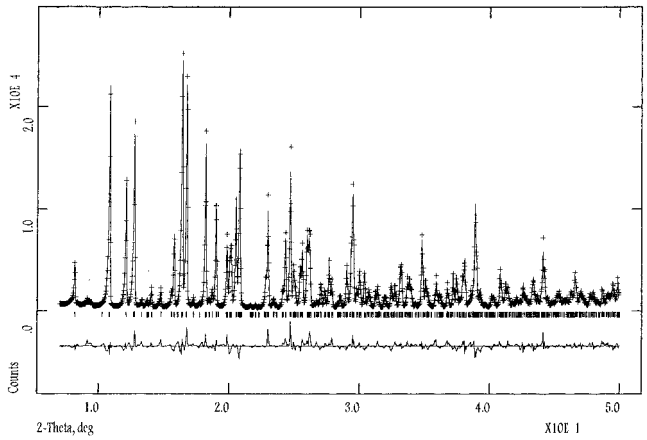

Figure 3. Rietveld refinement plot for δ-$(UO_2)_3(HO_3PC_6H_5)_2(O_3PC_6H_5)_2 \cdot H_2O$.

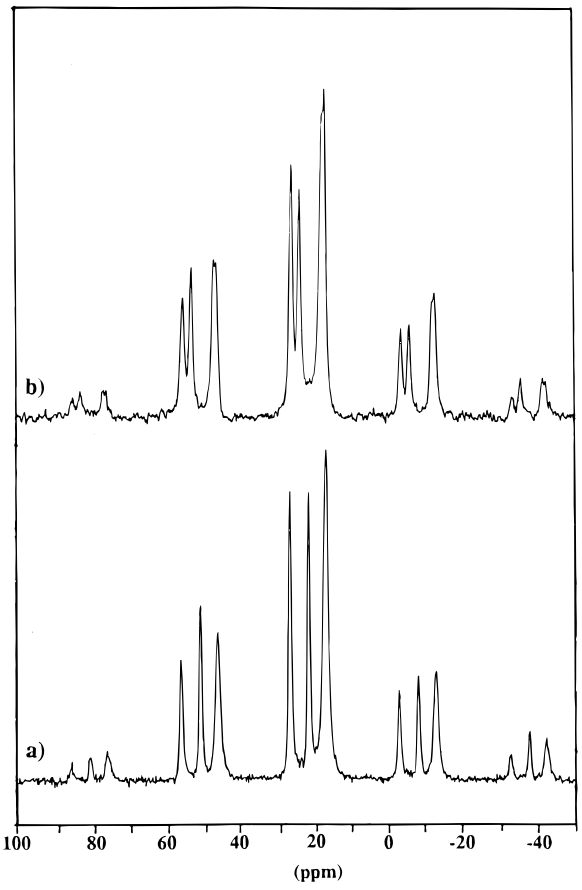

Figure 4. ^{31}P MAS NMR spectra for (a) δ-$(UO_2)_3(HO_3PC_6H_5)_2(O_3PC_6H_5)_2 \cdot H_2O$ and (b) ϵ-$(UO_2)_3(HO_3PC_6H_5)_2(O_3PC_6H_5)_2 \cdot H_2O$.

were kept fixed. These are reasonable crystallochemical values, and the quality of the pattern does not allow them to be refined.

The initial weighting factor for the soft constraints was −2000, and as the refinement progressed smoothly, this value was lowered. A value of −200 was used in the last refinement that converged to $R_{wP} = 13.1\%$, $R_F = 10.1\%$, with $a = 16.8268(7)$ Å, $b = 7.1673(8)$ Å, $c = 28.8228(12)$ Å, and $V = 3476.1(5)$ Å^3. The refined final atomic parameters for ϵ-UPP are given in Table 1, and bond distances, in Table 2. The final observed, calculated and difference profiles for ϵ-UPP are given in Figure 2. The same 2θ region was fitted for δ-UPP using the previously reported observed pattern, with the same determined structure[7] but using the new asymmetry correction for the

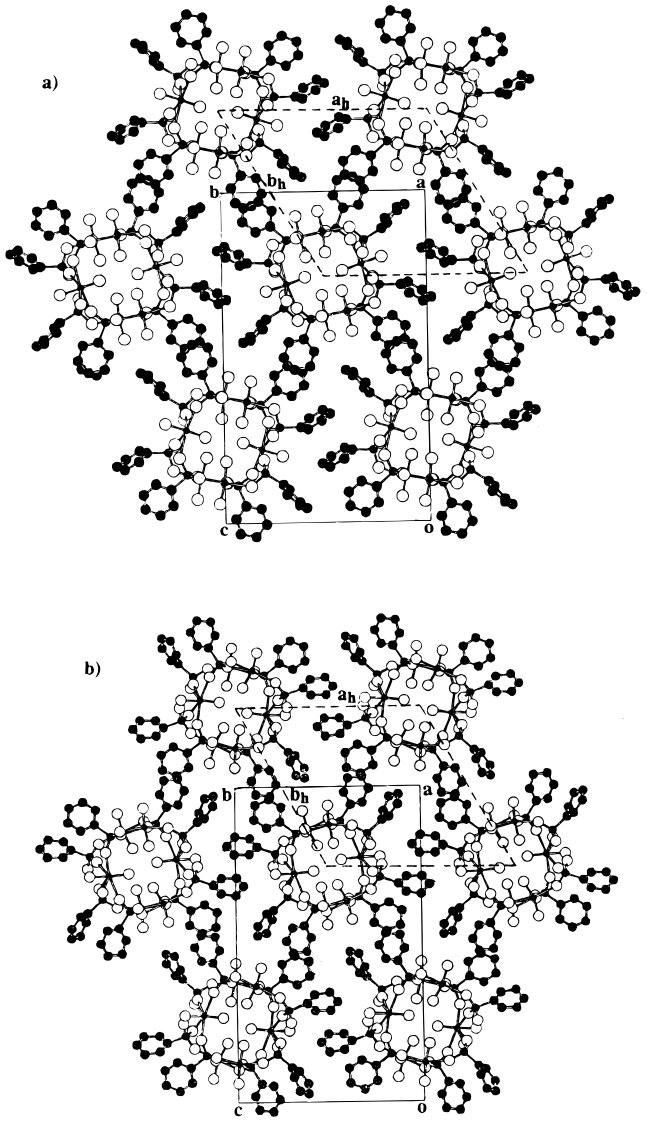

Figure 5. [010] view of the crystal structures for (a) δ-$(UO_2)_3(HO_3PC_6H_5)_2(O_3PC_6H_5)_2 \cdot H_2O$ and (b) ϵ-$(UO_2)_3(HO_3PC_6H_5)_2(O_3PC_6H_5)_2 \cdot H_2O$ showing the close packing of nanotubes. The pseudohexagonal lattice vectors are also shown.

diffraction peaks.[24] This resulted in an improvement of the fit, and R_{wP} fell from 12.9 to 10.8%. The final observed, calculated, and difference profiles for δ-UPP are given in Figure 3. The refined cell parameters were $a = 17.1839(2)$ Å, $b = 7.2076(2)$ Å, $c = 27.8018(4)$ Å, and $V = 3443.4(1)$ Å^3. The first peak at approximately 6° (2θ) had lower observed intensity, in both patterns, than that calculated with the proposed structures. This is very likely due to the X-ray beam being split out of the sample at such a low angle, and thus, this region has to be removed from the refinements.

^{31}P MAS NMR Study. The ^{31}P spectra for δ-UPP and ϵ-UPP are displayed in Figure 4a,b, respectively. The ^{31}P spectrum for δ-UPP is composed of the three main resonances and the corresponding satellite spinning bands. Two sharp peaks are located at 27.3 and 22.2 ppm, and the third broader one is situated at 17.4 ppm which has double integrated intensity. The ^{31}P spectrum for ϵ-UPP also shows a set of three main resonances, two located at 27.1 and 24.8 ppm and a third one at 18.1 ppm with double integrated intensity.

Scheme 1. Transformations between γ-, δ-, and ϵ-UPP

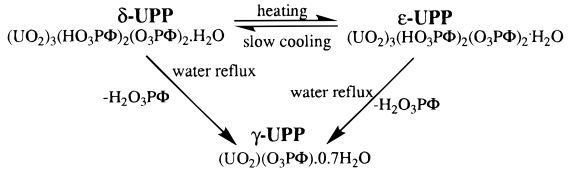

Discussion

The complete description of the tubular framework δ-UPP has been previously given.[7] The crystal structures of δ-UPP and ϵ-UPP, viewed down the *b*-axes, are displayed in Figure 5a,b, respectively. This view shows the close packing of nanotubes where six such tunnels surround a given one. This packing allows us to define a pseudo-hexagonal lattice and the corresponding lattice vectors are also displayed in Figure 5. It is important to underline that although the metric of the lattices are pseudohexagonal the symmetry is clearly orthorhombic. The nanotubes are held together by van der Waals forces between the phenyl rings. The pores are not quite circular being 7 × 6.5 Å for δ-UPP and 7 × 6.8 Å for ϵ-UPP. However these are the distances between the central walls of a nanotube and the free space is much lower due to the presence of the uranyl oxygens in the interior of the pores.

The dimensions of the pseudohexagonal lattice can be defined as a_h and b_h, and the relationships with the orthorhombic cell parameters are as follows: $a_h = a_o$ and $b_h = c_o/\sqrt{3}$. This results in $a_h = 16.83$ Å and $b_h = 16.64$ Å for ϵ-UPP and $a_h = 17.18$ Å and $b_h = 16.05$ Å for δ-UPP. The ϵ-phase is clearly more closely hexagonal than the δ-phase. This explains the results observed in the thermodiffractometric study, where split peaks for δ-UPP coalesce into main ones on heating. This is due to the overlapping of the peaks for the ϵ-phase (more closely hexagonal) where the values for a_h and b_h are so close that they do not allow these peaks to be resolved. This is a common result as high-temperature phases usually have more symmetry/order than the low-temperature phases.

In this case there are not symmetry changes at the phase transition. The transition δ-UPP → ϵ-UPP is topotactic as there are no bonds broken. Only a tilting of the groups to accommodate the nanotubes more efficiently is observed. The transition temperature is also quite low (≈150 °C) indicating very subtle distortions. The change of volume with temperature indicates a first-order phase transition as there is an abrupt change when the δ-phase transforms to the ϵ-phase. The thermodiffractometric study is indicative of a reversible phase transition, but ϵ-UPP phase can be isolated at room temperature by hydrothermal synthesis above 150 °C for a long period of time followed by "quenching" (cooling to room temperature at the atmosphere).

Heating δ-UPP (the low-temperature polymorph) at 170 °C for 4 h yields ϵ-UPP (the high-temperature polymorph). If this compound is cooled slowly from 170 °C to room temperature at 10 °C/h, the final solid is a mixture of both ϵ-UPP and δ-UPP phases. ϵ-UPP cooled slower, 3 °C/h, yields δ-UPP with a small amount of ϵ-UPP. The crystallinity of δ-UPP is lower due to smaller size of the microparticles that it results in broader diffraction peaks. The inherent overlapping of peaks in these very related phases, and the presence of broader diffraction peaks make difficult to determine quantitatively the amount of ϵ-UPP phase in the final samples. Probably, small microparticles of ϵ-UPP transform quickly while larger well-crystallized microparticles need much slower cooling to transform to δ-UPP. To accelerate this $\epsilon \rightarrow \delta$ transformation, ϵ-UPP was refluxed in water for 18 h. However, the resulting solid was γ-UPP, $UO_2(O_3PC_6H_5)\cdot 0.7H_2O$.[6] The transformations are summarized in Scheme 1. It is worthy to underline that the ϵ, $\delta \rightarrow \gamma$-UPP transformations are accompanied of a release of phenylphosphonic acid as the stoichiometries of these solids are different. Only at high P:U ratios are the ϵ- and δ-UPP phases stable in water.

Although this transition is reversible, the DTA curve on cooling does not display the thermal effect typical of a phase transformation. This behavior is due to the very slow kinetics, as in the usual working conditions, 5 °C/min = 300 °C/h, ϵ-UPP is effectively quenched. Very slow cooling rates, of the order of 1−2 deg/h, are needed to obtain δ-UPP, and this would result in a signal quite difficult to detect as it would be very spread.

ϵ-UPP obtained by hydrothermal synthesis has probably some pseudo-amorphous impurities as the background of the powder pattern shows some irregularities. This should also explain some differences in the chemical analysis of the sample. The

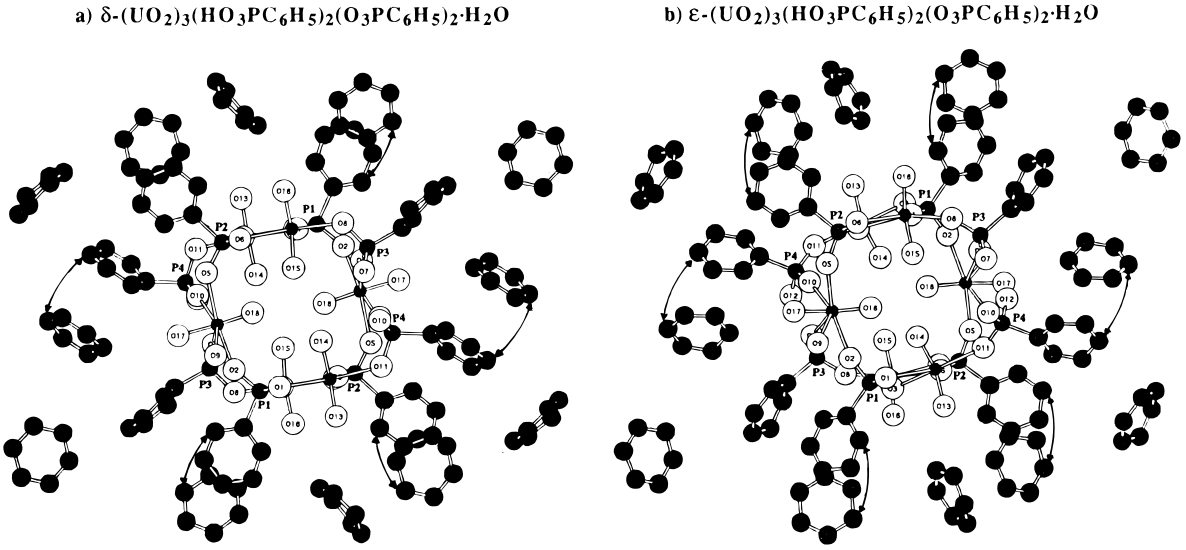

Figure 6. Enlarged view of a nanotube for δ-$(UO_2)_3(HO_3PC_6H_5)_2(O_3PC_6H_5)_2 \cdot H_2O$ and ϵ-$(UO_2)_3(HO_3PC_6H_5)_2(O_3PC_6H_5)_2 \cdot H_2O$ showing the phenyl groups that surround a given central nanotube with atoms labeled. The main van der Waals interactions between phenyl rings are outlined as solid lines.

determined elemental analysis for δ-UPP[7] agrees better with the $(UO_2)_3(HO_3PC_6H_5)_2(O_3PC_6H_5)_2 \cdot H_2O$ formula than that determined for ϵ-UPP.

The subtle observed structural changes in the δ to ϵ conversion affect all the groups. This is a molecular solid where nanotubes are only linked by weak van der Waals interactions. There is one main interaction between a central nanotube and each of the six nanotubes that surround it (along the *b* edge of the unit cell). These interactions are outlined in Figure 6a,b for δ-UPP and ϵ-UPP, respectively. Four of these interactions take place between the phenyl rings of P1 and P2 phosphonates. The other two interactions take place between the phenyl rings of the P4 phosphonates. The phenyl groups of the P3 phosphonate do not effectively participate in the interactions between nanotubes. The main difference between the two phases is the rotation of the P4 phenyl groups, causing a slight contraction along the *a*-axis and an expansion along the *c*-axis. The rotation of the phenyl rings, mainly P4, is clearly seen in Figure 6a,b. For instance, the U3−O(12) interaction is 2.96 Å in δ-UPP and 3.67 Å in ϵ-UPP. This rotation implies an energy barrier which makes possible to quench the metastable phase, ϵ-UPP, at room temperature.

The ^{31}P spectrum for δ-UPP has three bands due to the four crystallographically independent phosphorus atoms. The band at 17.4 ppm has double integrated intensity, and it must correspond to the signals due to P1 and P2 which are overlapped, i.e., the PO_3^{2-} groups. The ^{31}P signals for these type phosphonate groups are generally located at a lower chemical shift than those due to hydrogen phosphonate groups. A similar band is located at 18.1 ppm for ϵ-UPP also with double intensity. The overlapping is in agreement with the reported crystal structures as the environments around the two phosphorus atoms are very similar. The sharp bands located at 27.3 and 22.2 ppm for δ-UPP and at 27.1 and 24.8 ppm for ϵ-UPP must correspond to the hydrogen phosphonate groups. Moreover, the band at higher chemical shift must be associated with the P3 phosphorus as it almost does not change for the two phases and the phenyl groups bonded to this hydrogen phosphonate do not interact appreciably by van der Waals forces. The signal at 22.2 ppm for δ-UPP changes to 24.8 ppm for ϵ-UPP and therefore is probably due to the P4 phosphorus because of the different orientation of the P4 phenyl groups in the two structures. The main change observed in the structural study between the two polymorphs is the rotation of the P4 groups, and this is also the main change observed in the ^{31}P MAS NMR study.

Acknowledgment. We thank NATO for funding through the NATO CRG program No. 951242. The work in Málaga was supported by CICYT research grant PB 93/1245 of the Ministerio de Educación y Ciencia, Spain. A.C. thanks the R. A. Welch Foundation for partial support of this study under Grant No. A673.

IC9712941